Proton Shock Acceleration in Laser-Plasma Interactions

Luís O. Silva,* Michael Marti, Jonathan R. Davies, and Ricardo A. Fonseca
GoLP/Centro de Física dos Plasmas, Instituto Superior Técnico, 1049-001 Lisboa, Portugal

Chuang Ren, Frank S. Tsung, and Warren B. Mori
Department of Physics and Astronomy and of Electrical Engineering, University of California, Los Angeles, California 90095, USA

(Received 29 May 2003; published 8 January 2004)

The formation of strong, high Mach number (2–3), electrostatic shocks by laser pulses incident on overdense plasma slabs is observed in one- and two-dimensional particle-in-cell simulations, for a wide range of intensities, pulse durations, target thicknesses, and densities. The shocks propagate undisturbed across the plasma, accelerating the ions (protons). For a dimensionless field strength parameter $a_0 = 16$ ($I\lambda^2 \approx 3 \times 10^{20}$ W cm^{-2} μm^2, where I is the intensity and λ the wavelength), and target thicknesses of a few microns, the shock is responsible for the highest energy protons. A plateau in the ion spectrum provides a direct signature for shock acceleration.

DOI: 10.1103/PhysRevLett.92.015002 PACS numbers: 52.38.Kd, 52.35.Tc, 52.65.Rr

Present-day, state-of-the-art lasers can deliver ultraintense, ultrashort laser pulses, with intensities exceeding 10^{21} W cm^{-2}, with very high contrast ratios, in excess of 10^{10}:1. These systems can avoid the formation of plasma by the prepulse, thus opening the way to laser-solid interactions on ultrathin targets [1]. Recent experimental results show that ultraintense laser-solid interactions can produce proton beams, with potential applications in proton imaging and proton therapy. The possibilities opened up by intense lasers for proton acceleration have been explored in various experiments, but there is still debate about where the protons originate and about the acceleration mechanisms (for the conflicting views, see [2] versus [3], and for a review [4]).

In this Letter, we examine proton acceleration in the interaction of intense lasers with thin solid targets with particle-in-cell (PIC) simulations in one (1D) and two dimensions (2D). Our results allow us to identify two acceleration mechanisms: (i) proton acceleration due to the ambipolar fields arising in the free expansion of the strongly heated electrons at the front and rear of the target, and (ii) proton acceleration in a collisionless, electrostatic shock formed at the front of the target. Previous work has explored, via numerical simulations, the importance of sheath acceleration due to the plasma expansion at the rear side of the target, and have also observed the formation of solitary wave structures [5–8]. These nonlinear structures had low phase velocities (low Mach numbers $M \lesssim 1.6$), and were thus unable, by themselves, to accelerate ions to high energies. These studies used higher mass ions and/or lower intensities.

At higher laser intensities, and for thin targets ($\approx$2–11 μm), our simulations show that a different acceleration regime is present. We observe the formation of an electrostatic shock with a high Mach number $M = v_{\text{shock}}/c_s \simeq 2$–3, where v_{shock} is the shock velocity, and c_s is the local sound speed, with a laminar structure [9]. For a detailed discussion, see [9], and references therein. In addition, because of the intense heating of the background electrons by the incident laser, the effective sound speed is quite large; therefore c_s/c can exceed 0.1. This high velocity shock is responsible for the acceleration of the highest energy protons, with clear signatures in the proton spectrum and phase space.

We have performed a parametric scan for the interaction of a short laser pulse [full width at half maximum (FWHM) in the range $\tau_{\text{laser}} = 30$–500 fs] with an overdense target, with 1D and 2D PIC simulations, using OSIRIS framework [10], for a wide range of target thicknesses ($L_{\text{target}} = 0.1$–40 μm), incident laser intensities ($a_0 = 0.05$–20), and electron (proton) densities ($n_{e0} = 10$–$90 n_{\text{cr}}$, where n_{cr} is the critical density at which the laser frequency equals the electron plasma frequency). We carried out 1D (2D) simulations with 32 (16) particles per cell per species, with cell sizes of $\lambda_{e0}/10$ ($2\pi\lambda_{e0}/20$), where $\lambda_{e0} = c/\omega_{pe0} = \lambda_{pe0}/2\pi$ is the collisionless skin depth, with a laser pulse with a central wavelength $\lambda_0 = 2\pi c/\omega_0 = 1$ μm, propagating along the x_1 direction, and with a vacuum region of 80 μm (20 μm) on both sides of the target, with initial target electron (ion) temperature $T_e = 0$ keV ($T_i = 5$ keV). In 2D, the laser spot size was 5 μm or infinite (plane wave), and the transverse target dimension was 30 μm. In the simulations, distance is normalized to c/ω_0, time to $1/\omega_0$, charge to the electron charge e, and mass to the electron mass m_e.

For most of these conditions, the ponderomotive force of the laser launches an electrostatic, laminar shock from the front surface of the target, Fig. 1(a), and this nonlinear structure propagates almost undisturbed across the target, Fig. 1(c) and 1(d). The shock can then pick up ions,

 © 2004 The American Physical Society

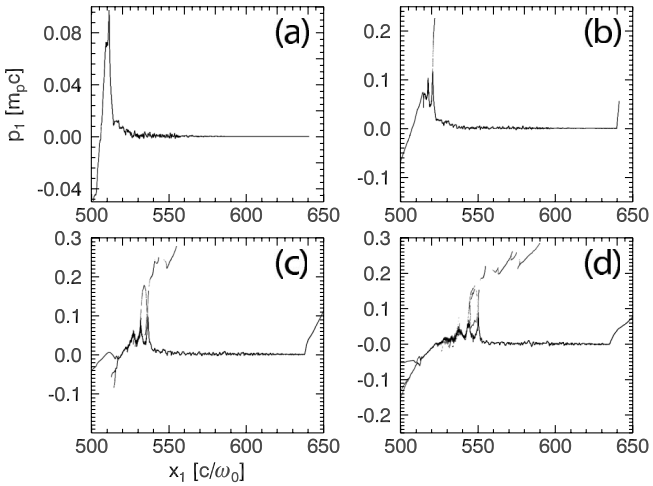

FIG. 1. Evolution of the ion phase space p_1x_1: (a) $t = 691.01/\omega_0$, (b) $t = 767.79/\omega_0$, (c) $t = 895.76/\omega_0$, (d) $t = 1023.72/\omega_0$. The cold target ($T_e = T_i = 0$) is initially located between $x_1 = 500c/\omega_0$ and $x_1 = 640c/\omega_0$. Target density is $n_{e0} = 10n_{cr}$, $a_0 = 16$, pulse duration $\tau_{laser} = 100$ fs, and target thickness is 21.8 μm.

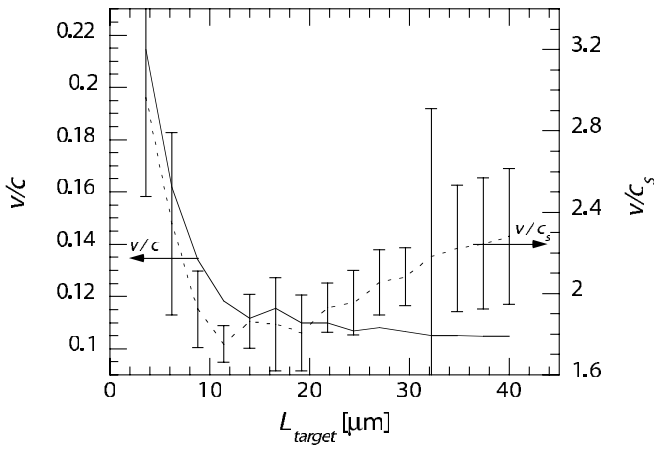

FIG. 2. Velocity of the shock as a function of the cold target thickness for $a_0 = 16$, $\tau_{laser} = 100$ fs, and $n_{e0} = 10n_{cr}$. The shock velocity is averaged over an interval of $255/\omega_0$, after the shock is formed. The formation time for these shocks is a few $2\pi/\omega_{pi0}$ [9]. (Solid line: shock Mach number; dashed line: shock velocity normalized to c.) Error bar in shock Mach number arises due to variation of c_s over the averaging time of the shock velocity.

Fig. 1(b), and reflect them to high energies ($\simeq 2v_{shock}$), Figs. 1(c) and 1(d). After the formation stage, the shock maintains a uniform velocity. The presence of an electrostatic, collisionless shock can be identified in the ion phase space p_1x_1, as illustrated in Fig. 1. The phase space structure is identical to the structures observed in the numerical piston-driven electrostatic shocks of Refs. [9]: the ions reflected off the shock provide the dissipation for shock formation, while the ions trapped behind the shock front [cf. Figs. 1(c) and 1(d)] dissipate the wavelike structure that forms behind the shock.

In our simulations, the laser field acts as a piston driving a flow of ions in the front surface moving into the target. Momentum conservation yields $(1 + \eta)I/c = m_i n_i v_i^2$, where I is the laser intensity, η is the laser reflection efficiency, and the momentum transferred to the electrons is discarded, since it is negligible in dense targets. The flow of ions has a velocity $v_{piston}/c = [(1 + \eta)I/m_i n_i c^3]^{1/2}$ [11]. The velocity of the ion piston determines the velocity of the shock. For turbulent shocks, such a piston can launch a shock close to the piston velocity only if the resulting shock Mach number is below the critical Mach number $M_c = 1.6$. For laminar shocks this limit is not present [9], and two critical Mach numbers are predicted. We have identified laminar shock structures with Mach numbers in the interval between the lower critical Mach number and the upper critical Mach number.

In Fig. 2, the measured shock velocity is plotted versus the target thickness while the laser amplitude (intensity) and pulse length were kept fixed at $a_0 = 16$ and $\tau = 100$ fs. This plot illustrates that both the absolute shock speed and Mach number are higher for thin targets and that the absolute speed decreases with target thickness. Therefore the highest energy ions are produced for the thinnest targets.

For "thin" targets, the target heats and begins to expand before the shock is formed. As noted in Ref. [9] the shock formation time is $\approx 2 \times 2\pi/\omega_{pi0}$ for $M \sim 1$ and $10 \times 2\pi/\omega_{pi0}$ for $M \cong 3.5$. Therefore, for targets thinner than $L_{target}/\lambda_0 \simeq 2\pi(2 - 10)v_{piston}/(\lambda_0\omega_{pi0}) = (2 - 10)(v_{piston}/c)(m_i/m_e)^{1/2}(n_{cr}/n_i)^{1/2}$, the shock propagates in the expanding plasma at the rear surface of the target, thus leading to even higher shock velocities in the laboratory frame. The expansion velocity of the rear surface is of the order of the local sound speed, and evolves with a typical time scaling of $(2\ln(\omega_{pi0}t))$ [12]. For "wider" targets, the heating time is longer. For high absolute shock speeds the electrons need to be uniformly heated. This requires electrons to be ponderomotively accelerated across the target and then to recirculate back to the front of the target as they are reflected from the sheath at the rear: a condition for large v_{shock}/c is that the shock formation time be longer than the recirculation time $L_{target}/\lambda_0 \lesssim (2 - 10)(m_i/m_e)^{1/2}(n_{cr}/n_i)^{1/2}/(2N_{e\text{-}cycle})$, where $N_{e\text{-}cycle}$ is the number of recirculations of the electron beam in the target. We have observed in both our 1D and 2D simulations that a single circulation cycle, $N_{e\text{-}cycle} = 1$, guarantees a uniform, and high, electron temperature in the shock formation region, and in the shock propagation region. The importance of electron recirculation on the acceleration in the sheath was discussed in Ref. [1].

The maximum velocity the target ions can pick up occurs for total reflection of the upstream ions in the

shock front, and it is simply given by $v_{\text{shock ions}} = 2v_{\text{shock}}$, independent of the mass and charge of the ions, where v_{shock} is the shock velocity. The maximum energy of the protons accelerated in the shock should then follow the shock velocity dependence with the target thickness. This is confirmed in Fig. 3, where for $a_0 = 16$ we observe a strong decrease in the proton energy up to $L_{\text{target}} \approx 10\ \mu$m, followed by a slower decrease from 10 to 20 μm, and an almost constant energy gain for $L_{\text{target}} \gtrsim 20\ \mu$m. Similar behavior is observed for lower intensities, consistent with the estimates outlined above. If the maximum energy of the protons in the shock is compared with the maximum energy of the protons accelerated at the rear surface of the target, then for high intensities, and relatively thin targets, proton shock acceleration is the mechanism responsible for the highest energy particles (Fig. 3).

Acceleration in the shock becomes the dominant acceleration mechanism, when the protons accelerated in the shock reach the sheath acceleration region at the rear side of the target with a higher velocity than the ions already accelerated in the sheath region. If we assume the electric field in the sheath region is constant over time scales comparable to the shock crossing time, and given by $E_{\text{sheath}} \sim k_B T_{\text{hot}}/e\lambda_D$, where λ_D is the Debye length of the hot electron component $\lambda_D = \sqrt{k_b T_{\text{hot}}/4\pi e^2 n_{\text{hot}}}$, T_{hot} (n_{hot}) is the temperature (density) of the hot electron component, and k_B is Boltzmann's constant, the maximum velocity the ions acquire in the sheath is given by $v_{\text{sheath ions}}(t) \approx ZeE_{\text{sheath}}t/m_i$, where t is the interaction time with the sheath. Shock acceleration becomes dominant when the velocity that ions gain in the shock is larger than the velocity ions can gain from acceleration in the sheath, i.e., $v_{\text{shock ions}} \approx 2v_{\text{shock}} \gtrsim v_{\text{sheath ions}}$. The time for the ions accelerated in the shock to reach the rear of the target is given by $t_{\text{crossing}} = L_{\text{target}}/2v_{\text{shock}}$; thus, when the ions accelerated in the shock reach the rear side of the target, the ions being accelerated in the sheath have already reached the velocity $v_{\text{sheath ions}} = ZeE_{\text{sheath}}L_{\text{target}}/2m_i v_{\text{shock}} = Zk_B T_{\text{hot}}L_{\text{target}}/2m_i v_{\text{shock}}\lambda_D$. Observing that $v_{\text{shock}} = Mc_s = M\sqrt{k_B T_{\text{hot}}/m_i}$ (and $k_b T_{\text{hot}}/m_e c^2 \approx 0.8a_0$ for 1 μm light, when $a_0 \gg 1$), the condition for shock-acceleration dominated scenarios ($v_{\text{shock ions}} \gtrsim v_{\text{sheath ions}}$) is $L_{\text{target}} \lesssim L_{\text{threshold}} = 4\lambda_D M^2/Z$. For thin targets, the shock acceleration dominates. It is important to stress that these simple scaling laws allow us to see that $M \simeq \sqrt{(1+\eta)/0.4}(n_{\text{cr}}/n_{\text{i0}})^{1/2}a_0^{1/2}$, for $a_0 \gg 1$, where we considered $v_{\text{shock}} \approx v_{\text{piston}}$. Two basic conditions must then be met: a high enough laser intensity to pistonlike drive the ions at the front side of the target to high Mach numbers, and strong electron heating in the shock formation region, in order to guarantee high c_s such that $v_{\text{piston}} \approx c_s$, thus guaranteeing a short shock formation time.

Since the acceleration process in the shock front for the highest energy ions is determined only by the shock velocity, which remains approximately constant, it is expected that a clear signature for this mechanism can be obtained in the ion spectrum. In Fig. 4, the temporal evolution of the ions in the simulation box shows the acceleration of the protons in a well-defined, narrow range, which then evolves to a plateau in the ion spectrum due to the further acceleration of the proton beam in the

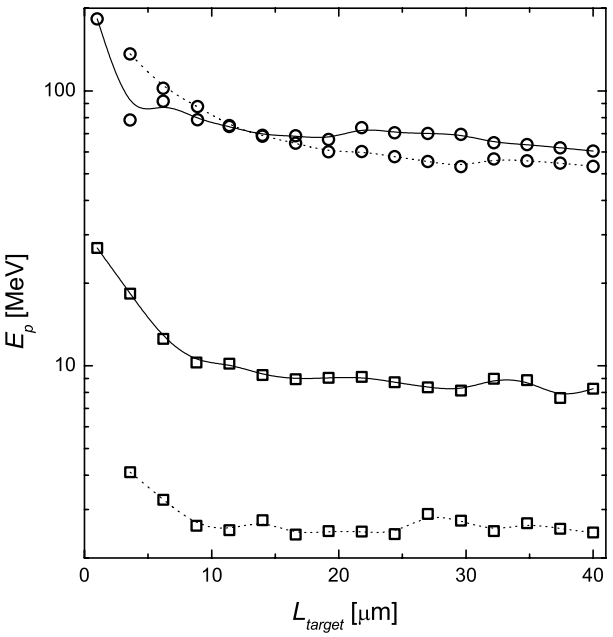

FIG. 3. Maximum proton energy as a function of cold target thickness and laser intensity for $n_{e0} = 10n_{\text{cr}}$, and $\tau_{\text{laser}} = 100$ fs (square: $a_0 = 4$; circle: $a_0 = 16$; dashed line: acceleration in the shock; solid line: acceleration in the rear of the target).

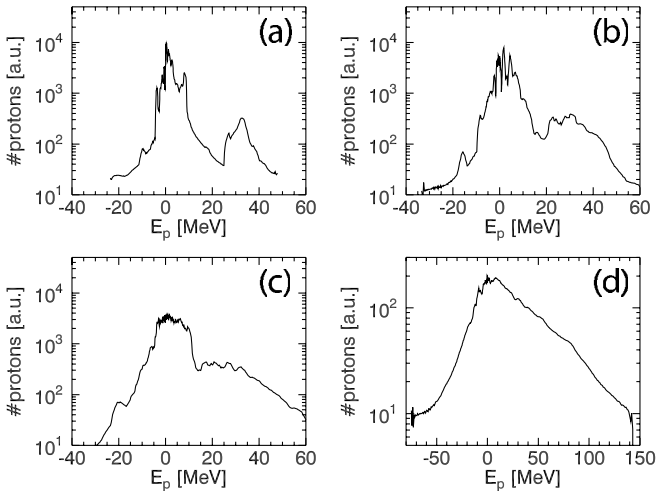

FIG. 4. Evolution of the ion spectrum: (a) $t = 998.13/\omega_0$, (b) $t = 1202.88/\omega_0$, (c) $t = 2290.58/\omega_0$, (d) $t = 1202.88/\omega_0$. $a_0 = 16$, $L_{\text{target}} = 8.8\ \mu$m for (a)–(c), $L_{\text{target}} = 1\ \mu$m for (d). Negative energies represent ions moving in the backward direction.

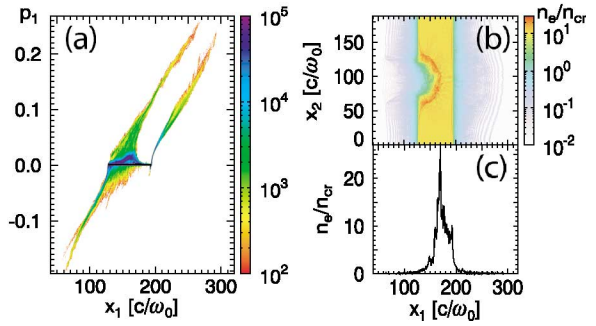

FIG. 5 (color). (a) Ion phase space p_1x_1, (b) electron density x_2x_1, and (c) lineout of the electron density (x_2 = const, along middle of the simulation box), from a 2D simulation, for $a_0 = 16$, $L_{\text{target}} = 11.4\ \mu$m, at $t = 884.81/\omega_0$. The two-dimensional sheath in both sides of the target is also evident.

sheath formed in the expanding plasma. The plateau in the ion spectrum is a direct signature for acceleration in the electrostatic shock launched by the laser. This signature has recently been identified in experimental results [13]. For high intensities and thin targets, the ions accelerated in this structure are also the most energetic ions (cf. Fig. 2). Furthermore, the density of energetic ions is significantly higher in the shock-acceleration mechanism, as previously pointed out in Ref. [7]. In general, the ion spectrum is a mixture of ions accelerated at the rear of the target and ions accelerated by the collisionless shock.

The above conclusions are based on 1D simulations. For a laser with a finite spot size the shock is not, in general, planar. To show these effects do not prevent the generation of high Mach number shocks, we have performed 2D PIC simulations, with equivalent parameters to the 1D simulations. The 1D and 2D simulations give, to within 5%, the same maximum proton energy, when measured for the same conditions (same distance from the target and same time after laser impact with the target) [14]. This is not surprising, since the highest energy protons are collinear with the laser pulse. In 2D simulations, when the target is irradiated either by a plane wave in the transverse direction or by a finite width spot, the shock structure is still identified in the ion phase space p_1x_1, and the ion spectrum. As shown in Fig. 5, when proton shock acceleration dominates in 1D it also prevails in 2D, with the ions accelerated in the shock front reaching higher energies than those accelerated at the rear surface of the target. The jump condition for the density across the shock front in 2D ($n_{\text{e,shock front}} \simeq 2.6 n_{\text{e,upstream}}$) also matches the theoretical and numerical predictions for high Mach number shocks [9]. When the laser spot size is wider, planar shocks are launched, the maximum energy of the ions is identical, and the signature in the ion spectrum is similar.

In conclusion, we have presented the first evidence, using 1D and 2D PIC simulations, for laminar, electrostatic, collisionless shocks with high Mach numbers, $M \approx 2$–3, driven by ultraintense lasers. Protons accelerated in the shock can reach higher energies than those accelerated at the rear side of the target: the range of parameters where proton shock acceleration dominates was identified, along with signatures in the ion spectrum for the presence of a collisionless shock. Our results indicate that state-of-the-art lasers now coming online are able to drive high Mach number collisionless shocks for the first time in the laboratory, thus opening the way to probe particle acceleration in collisionless shocks, a central problem in astrophysics. Furthermore, this acceleration mechanism opens new paths for the improvement of ion sources from intense laser-solid interactions. Taming these shocks, designing targets to improve coupling of the laser light to the shock, and optimizing the source of accelerated ions are future developments of this work.

This work was partially supported by FCT (Portugal) under Grants No. PESO/PRO/40144/2000, No. CERN/P/FIS/40132/2000, and No. POCTI/33605/FIS/2000, and by DOE under Grants No. DE-FG03-98DP00211 and No. DE-FC02-01ER41179, and by NSF under Grant No. NSF-PHY-0078508.

*Electronic address: luis.silva@ist.utl.pt

[1] A. J. Mackinnon *et al.*, Phys. Rev. Lett. **88**, 215006 (2002).
[2] E. L. Clark *et al.*, Phys. Rev. Lett. **84**, 670 (2000); A. Maksimchuk *et al.*, Phys. Rev. Lett. **84**, 4108 (2000); K. Nemoto *et al.*, Appl. Phys. Lett. **78**, 595 (2001).
[3] S. P. Hatchett *et al.*, Phys. Plasmas **7**, 2076 (2000); R. A. Snavely *et al.*, Phys. Rev. Lett. **85**, 2945 (2000); Y. Murakami *et al.*, Phys. Plasmas **8**, 4138 (2001); A. Pukhov, Phys. Rev. Lett. **86**, 3562 (2001).
[4] J. T. Mendonça *et al.*, Meas. Sci. Technol. **12**, 1801 (2001).
[5] J. Denavit, Phys. Rev. Lett. **69**, 3052 (1992).
[6] N. Izumi *et al.*, Phys. Rev. E **65**, 036413 (2002).
[7] A. Andreev *et al.*, Plasma Phys. Controlled Fusion **44**, 1243 (2002).
[8] A. Zhidkov *et al.*, Phys. Rev. Lett. **89**, 215002 (2002).
[9] D. W. Forslund and C. R. Shonk, Phys. Rev. Lett. **25**, 1699 (1970); D. W. Forslund and J. P. Freidberg, Phys. Rev. Lett. **27**, 1189 (1971).
[10] R. G. Hemker, Ph.D. thesis, UCLA, 2000; R. A. Fonseca *et al.*, *Lecture Notes in Computer Science* (Springer-Verlag, Heidelberg, 2002), Vol. 2329, p. III-342.
[11] S. C. Wilks *et al.*, Phys. Rev. Lett. **69**, 1383 (1992).
[12] P. Mora, Phys. Rev. Lett. **90**, 185002 (2003).
[13] M. Zepf *et al.*, Phys. Rev. Lett. **90**, 064801 (2003).
[14] M. Marti *et al.*, Bull. Am. Phys. Soc. **47**, 89 (2002).